L-mode to H-mode transition triggered by sawtooth-induced heat flux in EAST

L.M. Shao[1], G.S. Xu[1,2], N. Yan[1], R. Chen[1], L. Chen[1], Y.M. Duan[1], W. Gao[1], J. P. Qian[1], W. Shen[1], A. Ti[1], M. Xu[3], Q. Yu[4], L. Zhang[1], T. F. Zhou[1] and the EAST Team

[1] Institute of Plasma Physics, Chinese Academy of Sciences, Hefei 230031, People's Republic of China

[2] University of Science and Technology of China, Hefei 230031, People's Republic of China

[3] Southwestern Institute of Physics, PO Box 432, Chengdu 610041, People's Republic of China

[4] Max-Planck-Institut für Plasmaphysik, Boltzmannstr. 2, 85748 Garching, Germany

E-mail: shaolm@ipp.ac.cn

January 2019

Abstract.

H-modes induced by sawtooth events can be often obseverd in discharges with marginal auxiliary power injection in EAST. Poloidal flow shear at the very plasma edge, increasing ∼25% up to the threshold value, is observed just before the L-H transition by means of a fast reciprocating probe array in EAST. This suddenly risen poloidal flow shear, caused by the increased turbulent driven Reynolds force, is motived by the heat pulse originally released by a sawtooth crash at the plasma core. Associated with the critical poloidal flow shear, the local turbulent decorrelation rate increases significantly. The increased turbulent decorrelation rate compensated by nonlinear energy transfer rate from the turbulence to the low-frequency shear flows, exceeding the turbulence energy input rate, is sustained for several hundred microseconds till the turbulence quench happening.

1. Introduction

The low to high confinement mode transition (L-H transition) was first discovered at ASDEX in 1982 [1]. Since then a lot of scrape-off layer and divertor conditions have been considered for the L-H transition threshold power. These 'hidden conditions' include ∇B drift direction [2, 3, 4], Divertor compression [5], divertor magnetic geometry [6, 7, 8, 9], first wall materials [9, 10, 11], wall conditioning [12, 13], and so on. A condition of large sawtooth crashes at the plasma core triggering L-H or L-I transitions with reduced threshold power is also observed in EAST [14] and several other tokamaks [5, 15, 16, 17, 18]. The extremely fast, 'ballistic', sawtooth heat pulses, propagating from the plasma core to large minor radius within a few hundred microseconds, were reported in tokamaks of ORMAK [19, 20], TFTR [21, 22], DIII-D [21, 23], JET [24] and ASDEX Upgrade [25]. Sometimes, the heat pulse released by a sawtooth can stimulate an L-H transition when arriving at the plasma edge. However, the causal link between the sawtooth-induced heat pulse [21] and a spontaneous confinement regime transition is not fully understood.

Latest researchs show that there could be a radial electric field (and its shear) threshold value in the edge radial electric field well for the L-H transitions [26, 11, 27] and the ion channel of heat flux plays a key role [10, 28] on the confinement regime transitions. These key quanties are evaluated through a time slice of $\sim$ 10 ms, which is much longer than the time scale of an L-H transition (less than 1 ms). This means, while these dedicated experimental results make a great contribution to understand the plasma density dependent L-H transition threshold power, they do not point out the 'trigger' for the confinement regime transition. Previous studies show that turbulence-driven zonal-flows can act as the 'trigger' for the confinement regime transition [29, 30, 31, 32, 33, 34, 35, 36]. Especially, the rate of work done by the turbulent Reynolds stress has been considered as a critical term for driving the shear flow to large values [37, 32, 38, 33, 39], which can eventually result in a rapid turbulence suppression.

Recently, stationary zonal-flows in the edge E_{r} well are resolved by a high spatial resolution Doppler backscattering in the JET Ohmic and L-mode discharges [40]. However, the total estimated transferred power by Reynold stress is several times larger than the turbulence reduction from the gas puff imaging during the L-H transition in Alcator C-Mod [38, 33]. And, in some cases, the estimated transfer rate of energy from the turbulence into the shear flow is much smaller than the turbulence energy effective growth rate before the plasma entering the H-mode in EAST [41]. Therefore, more detailed investigations of the relationship between the energy reduce rate and energy growth rate of the local turbulence during the confinement regime transition are necessary. In this article, the role of turbulence-driven $E \times B$ flow shear on the turbulence collapse at the plasma edge is studied in a typical L-H transition discharge triggered by sawtooth-induced heat pulse in EAST.

The article is organized as follows. Section 2 gives a brief introduction to the discharges and key diagnostics used in this article. Section 3 introduces an example of L-H transitions triggered by a sawtooth event. The Dynamics of sawtooth heat pulse induced L-H transition

measured by a reciprocating probe array is illustrated in section 4. The discussion and conclusions are shown in the last section.

2. Discharge and diagnostic setup

To investigate the L-H transitions stimulated by a sawtooth-induced heat pulse, a series of discharges with low-power and zero torque RF (radio frequency)-dominent heating (~ 1 MW lower hybrid wave alone or combing with ~ 1 MW ion cyclotron resonance frequency), which is similar to the condition of the first phase of ITER plasmas [42], has been perform in the EAST tokamak. EAST is a medium-size superconducting tokamak run since 2006 with major and minor radii (R_0 and a) of 1.88 and 0.44 m, respectively. These discharges are run with a plasma current $I_\mathrm{p} = 400 - 600$ kA, core line-averaged density $n_\mathrm{e} = 2 - 4 \times 10^{19}$ m^{19}, toroidal magenetic field $B_\mathrm{T} = 1.8 - 2.0$ T, safty factor q_{95} of 3-5 and biased double null configuration ($dR_\mathrm{sep} = -1.5 - 1.5$ cm). Two typical sawtooth-induced L-H transition discharges #36030 and #42160 are presented in the following sections.

A multi-channel photodiodes system applied for studying fast dynamics of broadband plasma radiation was installed on EAST [43]. Linear arrays of silicon photon diodes encapsulated by pinhole cameras are utilized for absolute power measurement in the absolute extreme ultra violet (AXUV) spectral range. The lines of sight of the two pinhole cameras, each with 16 channels crossing the whole poloidal cross-section of the plasma, with spatial and temporal resolutions of $\sim$4.5 cm and 10 μs, are shown in figure 1 (a). The sensitive area of each photodiode channel is 2×5 mm^2 with a spacing of 0.12 mm between two channels. The fast AXUV diode system measures the plasma radiation between 1 eV and 6 keV [43], i.e., the spectral sensitivity covers a wide range of photon energies from the visible part of the spectrum up to the soft X-ray. In this paper channels just across the plasma edge, like d15 (blue line of sight) and u15 (cyan line of sight), are mostly used to identify an L-H transition.

A langmuir reciprocating probe diagnostic [44] located in the outer midplane is applied to measure some edge quantities during sawtooth-induced L-H transitions. Two kinds of probe heads are alone used in our dataset as shown in figures 1(b) and (c). The three-pins probe is used in discharge #36030 (see figure 2), while the two-dimensional probe array is applied in discharge #42160 (see figure 3). The diagram of the three-pins probe head with a diameter of 17 mm is shown in figure 1(b). The cylindrical graphite tips 1, 2 and 3 have a diameter of 2 mm as well as a length of 2 mm. Floating potentials are measured by tips 2 and 3 (ϕ_f2 and ϕ_f3) poloidally separated by 8 mm and the third tip 1 (ϕ_f1) in the middle of them. Tip 1, sticking out 8 mm of tips 2 and 3 in the radial direction, is located at $r - a = -12$ mm in this discharge #36030. The sampling rate of the diagnostic is up to 5 MHz with the data in a 12-bit digital resolution.

For better understanding the physics of L-H transition triggered by sawtooth-induced heat pulses, evolution of edge plasma parameters were measured by means of a two-dimensional reciprocating probe array with a temporal resolution of 1 μs as shown in figure 1(c). The probe tips are poloidally spaced by $dz = 6$ mm and radially spaced by

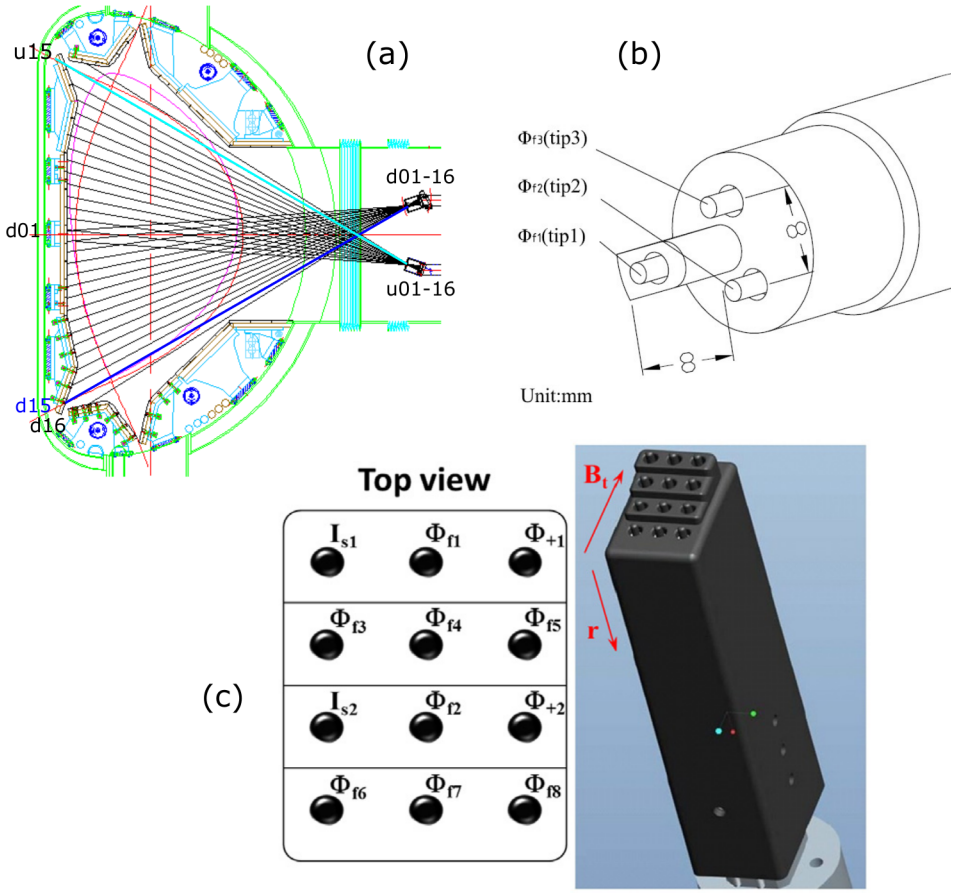

Figure 1: (a) The lines of sight of the AXUV diagnostic. (b) The diagram of the three-pins probe head applied to #36030. (c) Layout of 3×4 (poloidal $\times$ radial) probe array with tips poloidally spaced by $dz = 6$ mm and radially spaced by $dr = 2.5$ mm applied to #42160. Chordal view of channels d15 and u15 of the AXUV diagnostic are indicated in blue and cyan, respectively.

$dr = 2.5$ mm. All tips are 2 mm in length and 2 mm in diameter. Quantities $\phi_{\rm f1} - \phi_{\rm f8}$ and ϕ_{+1}/ϕ_{+2} are the floating potential and positively biased potential, respectively. Tips $I_{\rm s1}$ and $I_{\rm s2}$ measure the ion saturated current. Each 3-tips at the first ($I_{\rm s1}$, $\phi_{\rm f1}$, ϕ_{+1}) and third ($I_{\rm s2}$, $\phi_{\rm f2}$, ϕ_{+2}) layers form a triple probe, i.e., can provide electron density and temperature spontaneously. The innermost tips of the probe array are inserted into the plasma at $r - a = -5$ mm in discharge #42160.

3. L-H transition triggered by sawtooth heat pulse

Figure 2 shows an L-H transition heated by ~1.0 MW lower hybrid wave (LHW) of #36030. The plasma was run with current $I_{\rm p} = 600$ kA, core line-averaged density $\bar{n}_{\rm e} = 2.9 \times 10^{19}$ m^{-3}, toroidal field $B_{\rm T} = 1.88$ T, safety factor $q_{95} = 3.37$ and biased double null configuration ($dR_{\rm sep} = -1.0$ cm, the main active X-point is located in the lower divertor). Three sawtooth

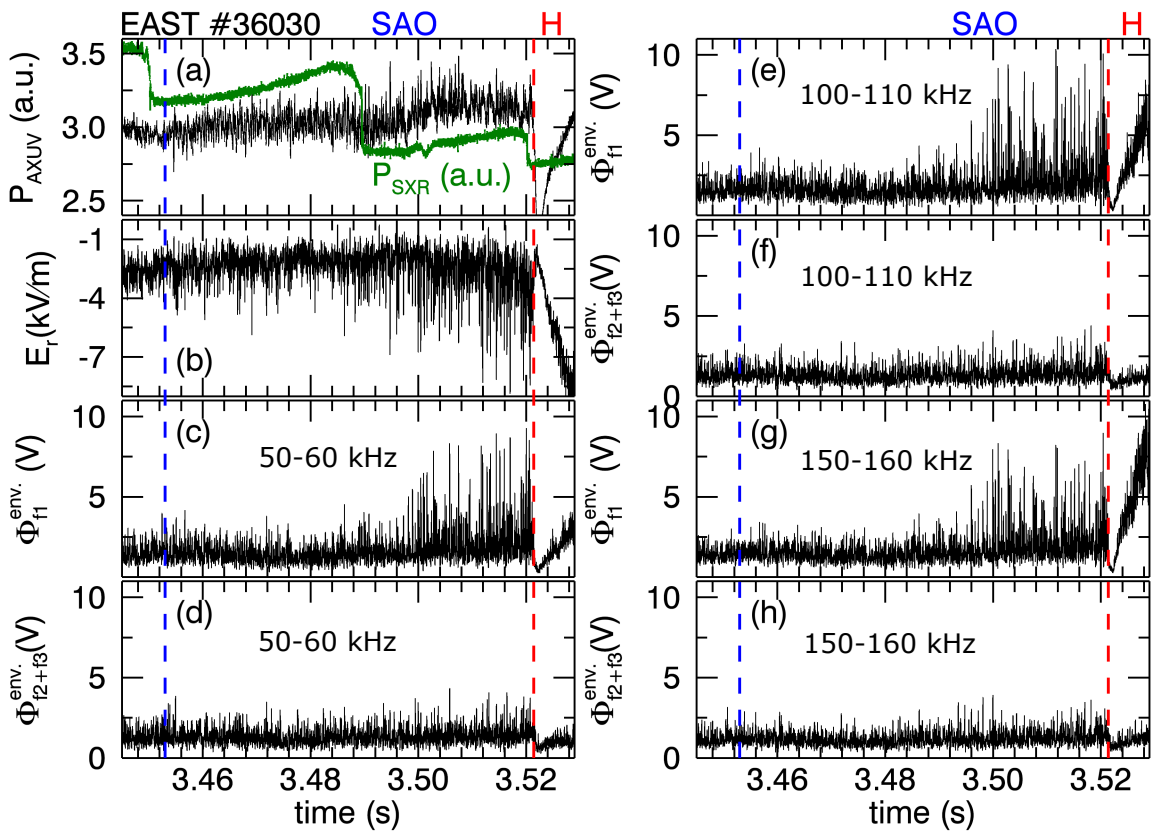

Figure 2: Typical sawtooth-induced L-H transition in EAST. (a) Edge AXUV signal of channel d15 and soft X-ray radiation across the plasma core, (b) Radial electric field at $r-a=-8$ mm, turbulence level in the frequency range of $50-60$ kHz at $r-a=-12$ mm (c) and -4 mm (d), turbulence level in the frequency range of $100-110$ kHz at $r-a=-12$ mm (e) and -4 mm (f) and turbulence level in the frequency range of $150-160$ kHz at $r-a=-12$ mm (g) and -4 mm (h) evaluated from a three-pins Langmuir probe measurements of #36030. The blue and red vertical dashed lines indicate the plasma entering the phase of small amplitude oscillations and H-mode, respectively.

crashes, resolved by a soft X-ray radiation across the plasma core (inside of $q=1$), are shown in figure 2(a). Small amplitude oscillations (SAOs) [45] at frequency of $\sim$3.5 kHz starting at 3.453 s, indicated by the blue vertical dashed lines, triggered by the first sawtooth crash, is revealed by the AXUV signal of channel d15 across the plasma edge (see figure 1(a)). Turbulence and flows interaction regulating the oscillations of SAOs has been reported in EAST recently [30, 45]. Here, no spectral filtration is applied to the detector of the AXUV diagnostic. The L-H transition, following the third sawtooth crash, occurs at 3.5214 s indicated by the red vertical dashed lines.

Shown in figure 2(b) is the radial electric field E_r at $r-a=-8$ mm evaluated as the

radial floating potential gradient (see figure 1(b)) instead of plasma potential gradient:

$$E_r = (\phi_{\rm f1} - \phi_{\rm f2+f3}/2)/\Delta r, \tag{1}$$

$$\phi_{\rm f2+f3} = \phi_{\rm f2} + \phi_{\rm f3}. \tag{2}$$

Here, we neglect the contribution from the gradient of the electron temperature to E_r. The inner and outer tips separately locate at the bottom and outboard edge of (bottom and outer part of) E_r well, which is reconstructed by the floating potential measurement of the inner tip during inserting into the edge plasma. The turbulence level $\Phi_{\rm f1}^{\rm env.}$ and $\Phi_{\rm f2+f3}^{\rm env.}$, the enveloped Hilbert transform of $\tilde{\phi}_{\rm f1}$ and $\tilde{\phi}_{\rm f2+f3}$ frequency filtered from 50 to 60 kHz, 100 to 110 kHz and from 150 to 160 kHz, separately at $r-a=-12$ and -4 mm, are shown in figures 2(c)-(h). The turbulence level is evaluated as,

$$\Phi_{\rm f1}^{\rm env.} = \sqrt{{\rm Hilbert}^2(\tilde{\phi}_{\rm f1}) + (\tilde{\phi}_{\rm f1})^2}, \qquad \tilde{\phi}_{\rm f1} = \phi_{\rm f1}^{50-60,100-110,150-160\ \rm kHz} \tag{3}$$

$$\Phi_{\rm f2+f3}^{\rm env.} = \sqrt{{\rm Hilbert}^2(\tilde{\phi}_{\rm f2+f3}) + (\tilde{\phi}_{\rm f2+f3})^2}, \quad \tilde{\phi}_{\rm f2+f3} = \phi_{\rm f2+f3}^{50-60,100-110,150-160\ \rm kHz}. \tag{4}$$

Here, band-pass filters within 50-60 kHz, 100-110 kHz and 150-160 kHz are applied to the input signals. About 6 ms after the second sawtooth crash, obviously larger peaks of turbulence level $\Phi_{\rm f1}^{\rm env.}$ are observed as shown in figures 1(c), (e), (g). Both turbulence levels $\Phi_{\rm f1}^{\rm env.}$ and $\Phi_{\rm f2+f3}^{\rm env.}$ in different frequency ranges are suppressed at the L-H transition as shown in figures 1(c)-(h). Same conclusion for turbulence levels is found in other narrow frequency ranges (every 10 kHz) within 20-250 kHz (not shown here). Nevertheless, no clear decrease of $E_{\rm r}$ at $r-a=-8$ mm is observed when the plasma approaching the H-mode.

4. Dynamics analysis at L-H transition

Figure 3 shows another sawtooth-induced L-H transition heated by LHW and ion cyclotron resonance frequency (ICRF) at respective source power of ∼1.5 and ∼0.9 MW of #42160. The plasma was run with $I_{\rm p}=0.4$ MA, $\bar{n}_{\rm e}\sim 2.3\times10^{19}$ m^{-3}, $B_{\rm T}=1.80$ T, $q_{95}=4.28$ and a biased double null configuration ($dR_{\rm sep}=1.5$ cm, the main active X-point located in the upper divertor) with ion ∇B drift upward. Shown in figures 3(a)-(d) are the edge AXUV signal of channel u15 (see figure 1(a)) and core electron cyclotron emission (ECE) inside of $q=1$, edge electron densities $n_{\rm e1}$ and $n_{\rm e2}$ at $r-a\sim-5.0$ and 0.0 mm, electron temperatures $T_{\rm e1}$ and $T_{\rm e2}$ at $r-a\sim-5.0$ and 0.0 mm, and electron pressure gradient $\nabla P_{\rm e}$ and negative poloidal flow shear $-\partial<v_\theta>/\partial r$ at $r-a\sim-2.5$ mm measured by the probe array (see figure 1(c)). The estimation of $n_{\rm e1}$ and $n_{\rm e2}$, $T_{\rm e1}$ and $T_{\rm e2}$, $\nabla P_{\rm e}$ and $-\partial<v_\theta>/\partial r$ can be seen in reference [45]. Before the L-H transition the average of edge electron density and temperature remain the same for ∼20 ms, while the mean of electron pressure gradient at $r-a=-2.5$ mm keeps the same over 50 ms. Two sawtooth events at 3.9621 and 3.9921 s are well revealed by the core ECE measurement in figure 3(a). 2.6 ms after the second sawtooth crash the plasma enters the H-mode indicated by the red vertical dashed line at 3.9947 s.

To investigate the role of sawtooth events on the L-H transition, two sawteeth in the time slice of 3.959-3.969 (first sawtooth event in figure 3) and 3.989-3.999 s (second sawtooth event

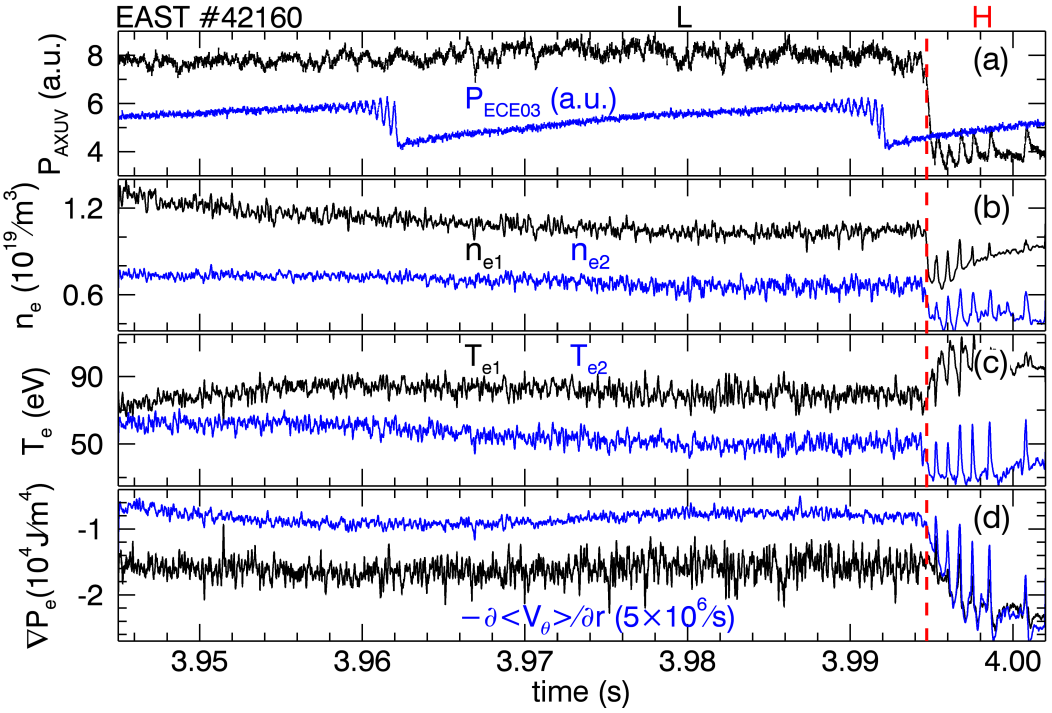

Figure 3: Time trace of (a) edge AXUV signal of channel u15 and core ECE emission inside of $q = 1$, (b) electron density n_{e1} and n_{e2} at $r - a \sim -5.0$ and 0.0 mm, (c) electron temperature T_{e1} and T_{e2} at $r - a \sim -5.0$ and 0.0 mm and (d) ∇P_e and $-\partial < v_\theta > /\partial r$ at $r - a \sim -2.5$ mm of #42160. The L-H transition is indicated by the red vertical dashed line at 3.9947 s.

in figure 3) are shown in figure 4. The turbulent level of electron density ($\Phi_{n_e}^{\text{env.}}$) frequency-filtered from 50 to 60 kHz and 100 to 110 kHz is evaluated as shown in figures 4(b) and (e). $\Phi_{n_e}^{\text{env.}}$ is calculated as,

$$\Phi_{n_e}^{\text{env.}} = \sqrt{\text{Hilbert}^2(\tilde{n}_{e1}) + (\tilde{n}_{e1})^2} \tag{5}$$

$$\tilde{n}_{e1} = n_{e1}^{50-60,100-110\ \text{kHz}}. \tag{6}$$

Here, band-pass filters covering the frequency rang of 50-60 and 100-110 kHz are applied to n_{e1}. After the plasma entering the H-mode, a clear drop of $\Phi_{n_e}^{\text{env.}}$ in figure 4(e) can be observed.

About 0.4 ms after the second sawtooth crash, the plasma enters the SAOs-phase at 3.9925 s indicated by the black vertical dashed line. Radial electric field at $r - a = -2.5$ mm in figure 4(f) is simply evaluated as the radial floating potential gradient, $E_r = (\phi_{f1} - \phi_{f2})/(2dr)$. The evaluated E_r, located at the outboard edge of E_r-well reconstructed by the floating potential measurement of ϕ_{f1}, are fairly comparable to $\nabla P_e/n_e e$ (here, $n_e = (n_{e1} + n_{e2})/2$) before the plasma entering the H-mode. The Doppler backscatering (DBS) diagnostic (recently developed) measurements show that the edge poloidal rotion is very small (several 0.1 km/s) in L-mode plasmas (without NBI heating) on EAST. We can infer that the $v \times B$ term has a little effect on the value of the electric field according to the radial force balance

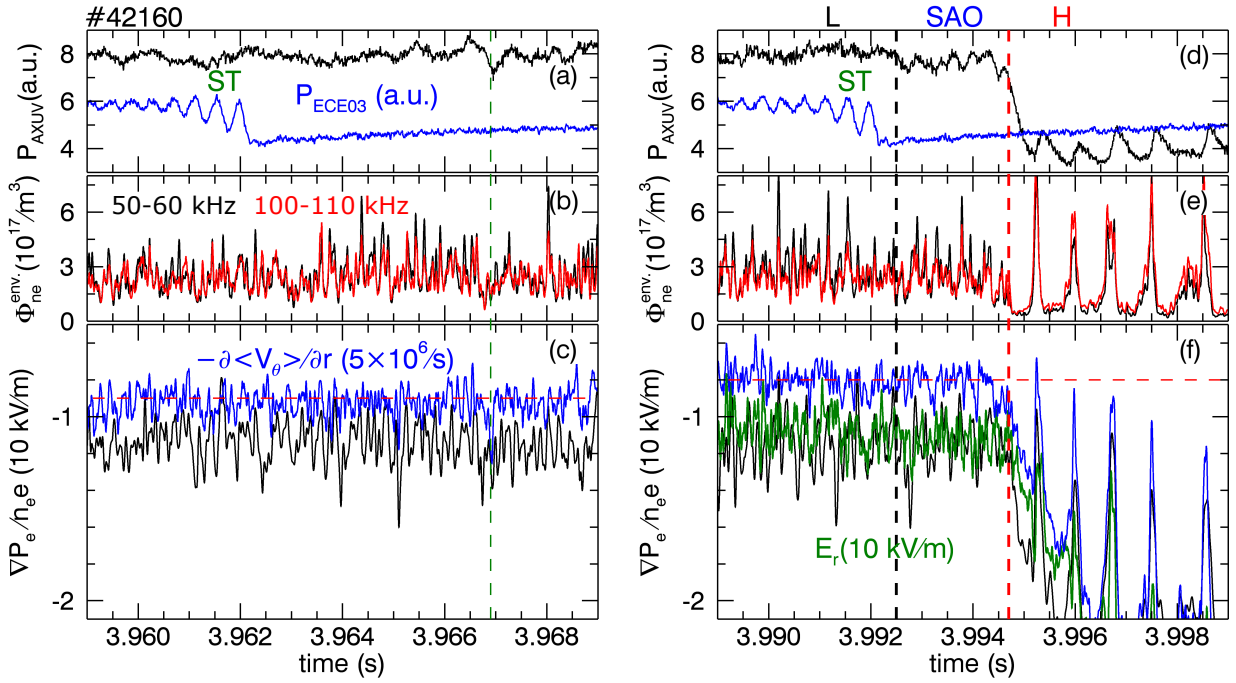

Figure 4: Time dependence of (a)/(d) edge AXUV signal of channel u15 and core ECE emission inside of $q = 1$, (b)/(e) turbulent level of electron density fluctuation $\Phi_{n_e}^{\text{env.}}$ frequency-filtered 50-60 kHz and 100-110 kHz at $r - a \sim -5.0$ mm and (c)/(f) $\nabla P_e/n_e e$ and $-\partial < v_\theta > /\partial r$ at $r - a \sim -2.5$ mm in the time slice of 3.959-3.969/3.989-3.999 s. The green vertical dashed line in (a)-(c) indicates a clear drop of edge AXUV signal. The green curve in (f) is E_r at $r - a \sim -2.5$ mm. The black vertical dashed line in (d)-(f) represents the plasma entering the SAOs phase at 3.9925 s.

equation, i.e., $E_r \approx \nabla P_i/n_i e$. Thus, it is reasonable to assume $\nabla P_e/n_e e \approx \nabla P_i/n_i e$, which is the neoclassical contribution to the radial electric field, at $r - a = -2.5$ mm before the L-H transition. However, in accordance with the observation in figure 2(b), no clear drop of E_r or $\nabla P_e/n_e e$ is discovered before the L-H transition.

Negative polodial flow shear $-\partial < v_\theta > /\partial r$ in the two time slices are respectively shown in figures 4(c) and (f). After some $\Phi_{n_e}^{\text{env.}}$ peaks, $\partial < v_\theta > /\partial r$ increases up to 5×10^6/s from $4.0 - 4.5 \times 10^6$/s as shown in panels 4(c) and (f). However, only at 3.9944 s, just before the L-H transition, the increased $\partial < v_\theta > /\partial r$ remains for ~300 μs (others are less than 100 μs). This suggests that the L-H transition ensues when $\partial < v_\theta > /\partial r$ reaches to its threshold value [29, 26, 35] and is sustained for an enough long time interval. Otherwise, the plasma will remain in L-mode. One case indicated by the green vertical dashed line is shown in figures 4(a)-(c).

For better understanding the dynamics of the L-H transition, flow energy transfer analysis in the time slice of 3.989-3.9965 s are shown in figures 5. ∇P_e and $-\partial < v_\theta > /\partial r$ at $r - a \sim -2.5$ mm as well as $\Phi_{n_e}^{\text{env.}}$ frequency-filtered 50-60 kHz and 100-110 kHz at $r - a \sim -5.0$ mm in figures 5(a) and (b) are adopted from figures 3(d) and 4(e). The green

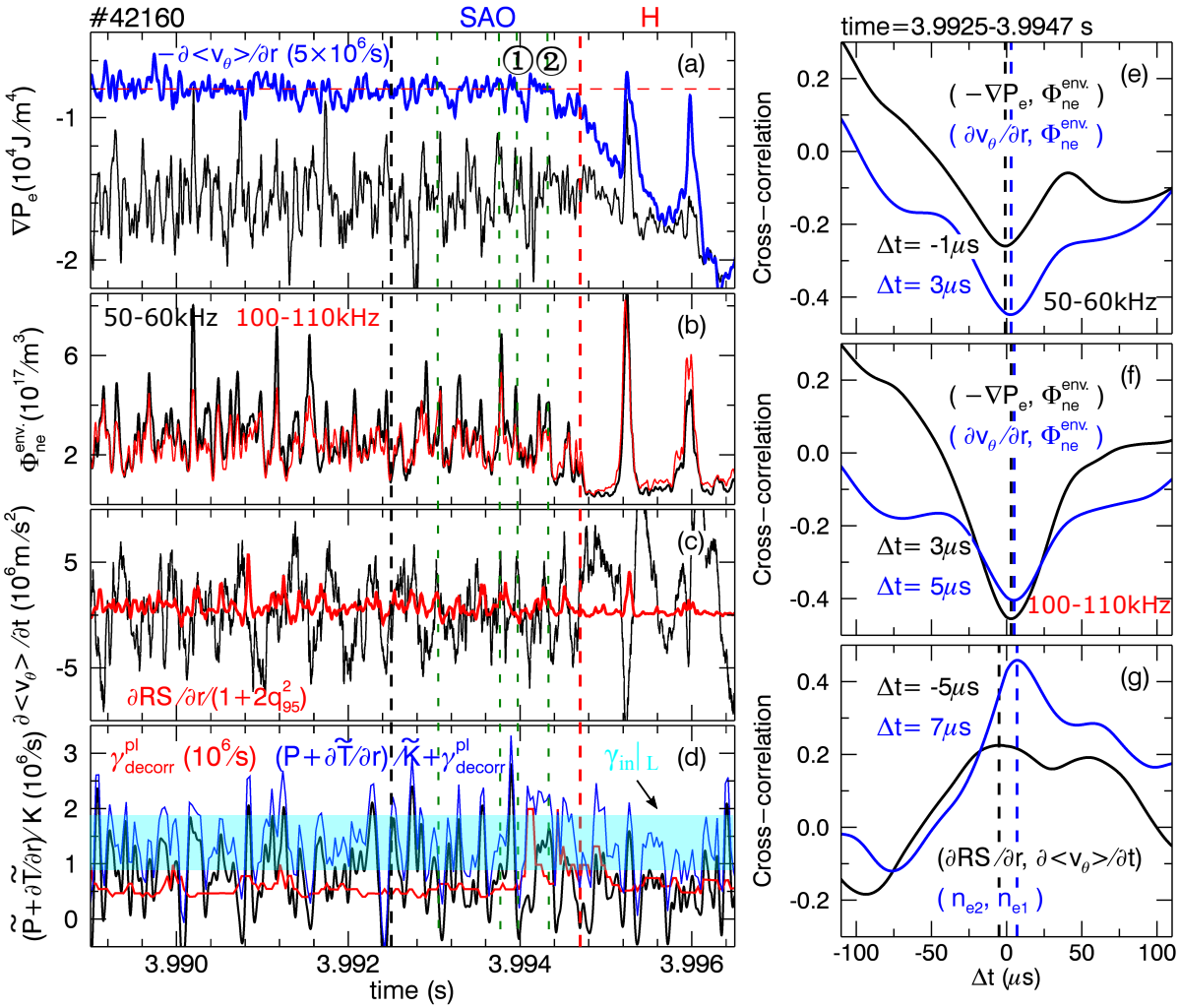

Figure 5: Time dependence of (a) $\nabla P_{\rm e}$ and $-\partial < v_\theta > /\partial r$ at $r-a \sim -2.5$ mm, (b) $\Phi^{\rm env.}_{n_{\rm e}}$ frequency-filtered 50-60 kHz and 100-110 kHz at $r-a \sim -5.0$ mm, (c) poloidal acceleration $\partial < v_\theta > /\partial t$ and Reynolds force with a factor of $1/(1+2q_{95}^2)$ at $r-a \sim -2.5$ mm and (d) energy transfer rate $\frac{P+\partial_r \tilde{T}}{\tilde{K}}$ into the $m, n = 0$ shear flow, plasma-frame turbulent decorrelation rate $\gamma^{\rm pl}_{\rm decorr}$ and their summation values at $r-a \sim -2.5$ mm. Cross correlations of (e) $-\nabla P_{\rm e}$ and $\partial < v_\theta > /\partial r$ with $\Phi^{\rm env.}_{n_{\rm e}}$ (50-60 kHz), (f) $-\nabla P_{\rm e}$ and $\partial < v_\theta > /\partial r$ with $\Phi^{\rm env.}_{n_{\rm e}}$ (100-110 kHz) and (g) $\partial <$ RS $> /\partial$r with $\partial < v_\theta > /\partial t$ and low-pass filtered $n_{\rm e2}$ with $n_{\rm e1}$ in the time slice of 3.9925-3.9947 s. The green vertical dashed lines in panels (a)-(d) indicate some peaks of $\Phi^{\rm env.}_{n_{\rm e}}$.

vertical dashed lines indicate some $\Phi^{\rm env.}_{n_{\rm e}}$ peaks in figure 5(b). After each $\Phi^{\rm env.}_{n_{\rm e}}$ peak in the SAOs-phase, associating with each SAOs oscillation, $\nabla P_{\rm e}$ deepens and $-\partial < v_\theta > /\partial r$ drops at $r-a \sim -2.5$ mm as shown in figure 5(a). An obvious drop of $\Phi^{\rm env.}_{n_{\rm e}}$ is observed as the plasma approaching the H-mode. However, no regular change (either increase or decrease) of $n_{\rm e}$ and $T_{\rm e}$ as well as their gradients is observed (not shown here).

One component of the poloidal acceleration driven by the Reynolds force $\partial < \mathrm{RS} > /\partial \mathrm{r}/(1+2\mathrm{q}_{95}^2)$ [46, 47] at $r-a \sim -2.5$ mm is shown in figure 5(c). The temporal evolution of $\partial < \mathrm{RS} > /\partial \mathrm{r}/(1+2\mathrm{q}_{95}^2)$, in accordance with $\Phi_{n_\mathrm{e}}^{\mathrm{env.}}$, is comparable to the poloidal acceleration $\partial < v_\theta > /\partial t$ at $r-a \sim -2.5$ mm during the SAOs. The estimation of $\partial < v_\theta > /\partial t$ and Reynolds stress gradient $\partial < \mathrm{RS} > /\partial \mathrm{r}$ is shown below,

$$\partial < v_\theta > /\partial t = \partial < \phi_{\mathrm{f2}} - \phi_{\mathrm{f1}} > /\partial t/(2drB_\mathrm{T}) \tag{7}$$

$$\partial < \mathrm{RS} > /\partial r = [< (\tilde{\phi}_{\mathrm{f2}} - \tilde{\phi}_{\mathrm{f4}})(\tilde{\phi}_{\mathrm{f5}} - \tilde{\phi}_{\mathrm{f4}}) > - < (\tilde{\phi}_{\mathrm{f4}} - \tilde{\phi}_{\mathrm{f1}})(\tilde{\phi}_{\mathrm{f5}} - \tilde{\phi}_{\mathrm{f4}}) >]/[dz(drB_\mathrm{T})^2] \tag{8}$$

$$\tilde{\phi}_{\mathrm{f1}} = \phi_{\mathrm{f1}}^{30-250\ \mathrm{kHz}}, \quad \tilde{\phi}_{\mathrm{f2}} = \phi_{\mathrm{f2}}^{30-250\ \mathrm{kHz}}, \quad \tilde{\phi}_{\mathrm{f4}} = \phi_{\mathrm{f4}}^{30-250\ \mathrm{kHz}}, \quad \tilde{\phi}_{\mathrm{f5}} = \phi_{\mathrm{f5}}^{30-250\ \mathrm{kHz}}. \tag{9}$$

Here, a band-pass filter covering the frequency range from 30 to 250 kHz is applied to floating potential ϕ_{f1}, ϕ_{f2}, ϕ_{f4} and ϕ_{f5}, since the contribution to the Reynolds stress is mainly from the turbulence in the frequency range of 30-250 kHz. And a low-pass filter (< 10 kHz) is utilized to evaluate the Reynolds stress < RS >. There is almost no time delay between $\partial < v_\theta > /\partial t$ and $\partial < \mathrm{RS} > /\partial \mathrm{r}$ in the time slice of 3.9925-3.9947 s evaluated by the normalized cross-correlation function [48] as shown in figure 5(g).

The cross correlations of the negative pressure gradient $-\nabla P_\mathrm{e}$ and poloidal flow shear $\partial < v_\theta > /\partial r$ with edge turbulence level $\Phi_{n_\mathrm{e}}^{\mathrm{env.}}$ frequerncy-filetered 50-60 and 100-110 kHz in the SAOs-phase (3.9925-3.9947 s) are shown in figures 5(e) and (f), respectively. Here, the reference signals are $\Phi_{n_\mathrm{e}}^{\mathrm{env.}}$. Both $\Phi_{n_\mathrm{e}}^{\mathrm{env.}}$ (50-60 kHz) and $\Phi_{n_\mathrm{e}}^{\mathrm{env.}}$ (100-110 kHz) are reversely correlated with $-\nabla P_\mathrm{e}$ and $\partial < v_\theta > /\partial r$, i.e., $\Phi_{n_\mathrm{e}}^{\mathrm{env.}}$ preceding $-\nabla P_\mathrm{e}$ and $\partial < v_\theta > /\partial r$ around π in phase. Note here, we should take the propagating time of the heat flux from $r-a=-5$ to -2.5 mm into account. Figure 5(g) shows that the delay time between low-pass filtered $n_{\mathrm{e}2}$ at $r-a=-5$ mm and $n_{\mathrm{e}1}$ (reference signal) at $r-a=0$ mm is 7 μs. Since each oscillation of SAOs has an averaged period of 304 μs, we can infer that the propagating time of the heat flux from $r-a=-5$ to -2.5 mm can be neglected comparing to the averaged period of SAOs. Therefore, at $r-a=-2.5$ mm, the turbulent fluctuation of electron density precedes $-\nabla P_\mathrm{e}$ and $\partial < v_\theta > /\partial r$ about π in phase, which is consistent with the Kim-Diamond model of turbulence and zonal-flows interaction [29, 49] where the limit cycle oscillation (LCO) phase delay between the turbulence and zonal-flow shear increase from $\sim \frac{\pi}{2}$ to $\sim \pi$ as the plasma approaching the H-mode.

In recent experimental investigations [38, 33, 35], a criterion for the onset of fast turbulence suppression due to its nonlinear transfer of kinetic energy into the sheared $E \times B$ flow is expressed as,

$$R_\mathrm{T} \equiv \frac{P + \partial_r \tilde{T}}{(\gamma_{\mathrm{in}} - \gamma_{\mathrm{decorr}}^{\mathrm{pl}})\tilde{K}} > 1, \tag{10}$$

where the notations are given as

$$P = < \tilde{v}_\mathrm{r}\tilde{v}_\theta > \frac{\partial < v_\theta >}{\partial r}, \tag{11}$$

$$\tilde{T} = < \tilde{v}_\mathrm{r}\tilde{v}_\theta^2 >, \tag{12}$$

$$\tilde{K} = \frac{1}{2} < \tilde{v}_\mathrm{r}^2 + \tilde{v}_\theta^2 >, \tag{13}$$

$$\gamma_{\rm in} = \gamma_{\rm in}(\nabla n, \nabla T, < v_\theta >'), \tag{14}$$

$$\gamma^{\rm pl}_{\rm decorr} = \sqrt{\gamma^2_{\rm decorr}|_{\rm lab} - (< v_\theta > /L^{\rm corr}_\theta)^2}. \tag{15}$$

Here, P is the nonlinear turbulent production of shear flow, $\tilde{T}$ is the radial turbulent intensity flux, $\tilde{K}$ is the kinetic energy on the fluctuation, $\gamma_{\rm in}$ and $\gamma^{\rm pl}_{\rm decorr}$ denote the turbulence growth rate driven by the underlying instability and the effective rate of turbulent decorrelation due to high-frequency dissipation effects, respectively. And, $L^{\rm corr}_\theta$ is the poloidal turbulence correlation length of turbulence.

Nonlinear kinetic energy transfer rate $\frac{P+\partial_r\tilde{T}}{\tilde{K}}$ from turbulence into the $m, n = 0$ $E \times B$ shear flow and plasma-frame turbulent decorrelation rate $\gamma^{\rm pl}_{\rm decorr}$ as well as their summation values ($\frac{P+\partial_r\tilde{T}}{\tilde{K}} + \gamma^{\rm pl}_{\rm decorr}$) at $r - a = -2.5$ mm are shown in figure 5(e). Here, we apply $\tilde{v}_{\rm r} = v^{30-250\ \rm kHz}_{\rm r1}$ and $\tilde{v}_\theta = (\phi^{30-250\ \rm kHz}_{\rm f4} - \phi^{30-250\ \rm kHz}_{\rm f1})/(drB_{\rm T})$ to the estimation of $\frac{P+\partial_r\tilde{T}}{\tilde{K}}$. The turbulence decorrelation rate in the laboratory frame is calculated as $\gamma_{\rm decorr}|_{\rm lab} = \frac{1}{\tau_{\rm cc}}$, where the cross-correlation time $\tau_{\rm cc}$ is evaluated by the method of cross-correlation between $\phi^{50-250\ \rm kHz}_{\rm f4}$ with $\phi^{50-250\ \rm kHz}_{\rm f5}$. Here, we apply a band-pass filter covering the frequency range from 50 to 250 kHz to floating potential $\phi_{\rm f4}$ and $\phi_{\rm f5}$ when evaluating the turbulence decorrelation time, because the turbulence in the frequency range of 50-250 kHz well meets the condition of high-frequency dissiption in this discharge. Local wavenumber and frequency spectral density $S_l(k, f)$ in the time slice of 3.960-3.994 s can be calculated from probe pairs $\phi_{\rm f4}$ and $\phi_{\rm f5}$ using the two-point correlation technique [50, 51]. Then the poloidal turbulence correlation length of turbulence in the frequency range of 50-250 kHz can be evaluated ($L^{\rm corr}_\theta = 3.25$ cm). Since the L-mode state between the two sawtooth events is temporal stationary, we can estimate the turbulence energy input rate at $r - a = -2.5$ mm in the stationary L-mode (3.982-3.992 s) as,

$$\gamma_{\rm in}|_{\rm L} = \gamma^{\rm pl}_{\rm decorr}|_{\rm L} + \frac{P+\partial_r\tilde{T}}{\tilde{K}}|_{\rm L} \approx 0.9 - 1.9 \times 10^{-6}\ {\rm s}^{-1}. \tag{16}$$

The errorband for the turbulence energy input rate is calculated from the standard deviation in the time slice of 3.982-3.992 s. Just before the L-H transition $\gamma^{\rm pl}_{\rm decorr}$ sharply goes up, corresponding to $\partial < v_\theta > /\partial r$ increasing from ~ 4 up to $\sim 5 \times 10^6$/s, indicated by two green vertical dashed lines labelled as ① and ②. The increased $\gamma^{\rm pl}_{\rm decorr}$ compensated by $\frac{P+\partial_r\tilde{T}}{\tilde{K}}$ over the turbulence energy input rate $\gamma_{\rm in}|_{\rm L}$, i.e., $\gamma^{\rm pl}_{\rm decorr} + \frac{P+\partial_r\tilde{T}}{\tilde{K}} > \gamma_{\rm in}|_{\rm L}$, is sustained for ~ 500 μs till the plasma enters the H-mode. This suggests that both $\gamma^{\rm pl}_{\rm decorr}$ and $\frac{P+\partial_r\tilde{T}}{\tilde{K}}$ play an important role on the rapid turbulence suppression at the marginal power injection. Although there are some cases with turbulence energy loss rate ($\gamma^{\rm pl}_{\rm decorr} + \frac{P+\partial_r\tilde{T}}{\tilde{K}}$) up to its threshold value ($\gamma_{\rm in}|_{\rm L}$) for ~ 100 μs, no L-H transition is observed. Therefore, we can infer that at the critical shear rate of poloidal flow the turbulence quench ensues when the turbulence energy loss rate is up to its threshold value and sustained for an enough long time interval. Otherwise, the turbulence will recover.

5. Discussion and Conclusions

In this paper the causal link between the sawtooth-induced heat pulses at the plasma edge and a spontaneous L-H transition is proposed. Just before the L-H transition, as the sawtooth-induced heat pulse propagates outward the very plasma edge is left with a steeper pressure gradient and a larger poloidal flow shear (up to the threshold value). Associated with the critical poloidal flow shear, the turbulent decorrelation rate $\gamma^{\rm pl}_{\rm decorr}$ sharply goes up. The ramp-up $\gamma^{\rm pl}_{\rm decorr}$ compensated by nonlinear energy transfer rate $\frac{P+\partial_r\tilde{T}}{\tilde{K}}$ from the turbulence to the $E\times B$ shear flow is over the turbulence energy input rate $\gamma_{\rm in}$ and sustained for several 100 μs. As a consequence, the turbulence quench happens. As soon as the plasma enters the H-mode the pressure gradient will steepen up, which increases the neoclassical contribution. We also find that the turbulence level recovers when the turbulence reduction rate ($\frac{P+\partial_r\tilde{T}}{\tilde{K}}+\gamma^{\rm pl}_{\rm decorr}$) reaches to its threshold value while is not sustained for an enough long time interval.

As mentioned in the 'Introduction' section, in DIII-D and Alcator C-Mod tokamaks, the total estimated transferred power from different edge diagnostic measurements is observed to be several times larger than the turbulence reduction during L-H transitions [37, 32, 38, 33]. In these estimations the turbulence effective growth rate $\gamma_{\rm eff}=\gamma_{\rm in}-\gamma^{\rm pl}_{\rm decorr}$ is assumed to be a constant value. However, in this article, $\gamma^{\rm pl}_{\rm decorr}$ is found to increase significantly just before the confinement regime transition as the poloidal flow shear is up to its threshold value. Thus, we assume $\gamma_{\rm in}$ keeping the same before the L-H transition. And, just before the L-H transition, the total estimated turbulence loss rate and the turbulence energy input rate are found to be similar at the very plasma edge in EAST.

Many conditions have impact on L-H transition threshold power as presented in the 'Introduction' section. Since some conditions need to be changed for achieving an L-H transition discharge without sawteeth, we can not make a conclusion that the threshold power would be higher in non-sawtoothing discharges, although large sawtooth lowering the threshold power is observed. Nevertheless, the stimulated heat pulses released by sawteeth or (1,1) fishbone mode bursts in neutral beam injection discharges could be a potential technique for stimulating an underpowered plasma into H-mode.

There is no edge ion temperature and pressure profile measurements, therefore, we assume electron pressure gradient equal to ion pressure gradient at the plasma edge before the L-H transition in this paper. The poloidal flow shear at the very plasma edge increasing $\sim 25\%$ with the contribution of Reynolds force just before the L-H transition suggests that the ion pressure profile creates $\sim 75\%$ of the poloidal flow shear, i.e., playing a major role on the formation of $E_{\rm r}$ shear. The causal link between the sawtooth-induced heat pulses at the plasma edge and a spontaneous L-H transition proposed in this article is consistent with the Kim-Diamond model of turbulence and zonal-flows interaction [29, 49]. However, the impact of the sawtooth-induced ion heat pulses, which propagate slower than the electron sawtooth heat pulses [21], on the creation of increased $E_{\rm r}$ shear just before the L-H transition is unclear. Distinguishing the roles of the electron and ion sawtooth heat pulses on the confinement regime transition will be a subject of the future investigations.

Acknowledgments

The authors would like to thank G. Birkenmeier, Z.P. Luo, P. Manz, H.Q. Wang and E. Wolfrum for constructive discussions. This work was supported by National Magnetic Confinement Fusion Science Program of China under Contracts No. 2015GB101000, National Key Research and Development Program of China No. 2017YFE0300402, National Natural Science Foundation of China under Contract No.11805238, No.11575235 and No.11575248 and CASHIPS Director's Fund, Grant No.YZJJ2018QN9.

References

[1] F. Wagner, G. Becker, K. Behringer, D. Campbell, A. Eberhagen, W. Engelhardt, G. Fussmann, O. Gehre, J. Gernhardt, G. v. Gierke, G. Haas, M. Huang, F. Karger, M. Keilhacker, Q. Klüber, M. Kornherr, K. Lackner, G. Lisitano, G. G. Lister, H. M. Mayer, D. Meisel, E. R. Müiller, H. Murmann, H. Niedermeyer, W. Poschenrieder, H. Rapp, H. Röhr, F. Schneider, G. Siller, E. Speth, A. Stäbler, K. H. Steuer, G. Venus, O. Vollmer, and Z. Yü, Phys. Rev. Lett. **49**, 1408 (1982).

[2] ASDEX-Team, Nucl. Fusion **29**, 1959 (1989).

[3] B. LaBombard, J. E. Rice, A. E. Hubbard, J. W. Hughes, M. Greenwald, R. S. Granetz, J. H. Irby, Y. Lin, B. Lipschultz, E. S. Marmar, K. Marr, D. Mossessian, R. Parker, W. Rowan, N. Smick, J. A. Snipes, J. L. Terry, S. M. Wolfe, S. J. Wukitch, and the Alcator C-Mode Team, Phys. Plasmas **12**, 056111 (2005).

[4] H. Meyer, A. R. Field, R. J. Akers, C. Brickley, N. J. Conway, A. Patel, P. G. Carolan, C. Challis, G. F. Counsell, G. Cunningham, P. Helander, A. Kirk, B. Lloyd, R. Maingi, M. R. Tournianski, M. J. Walsh, and the MAST and NBI teams, Plasma Phys. Control. Fusion **46**, A291 (2004).

[5] F. Wagner, Plasma Phys. Control. Fusion **49**, B1 (2007).

[6] Y. Andrew, N. C. Hawkes, M. G. O'Mullane, R. Sartori, M. de Baar, I. Coffey, K. Guenther, I. Jenkins, A. Korotkov, P. Lomas, G. F. Matthews, A. Matilal, R. Prentice, M. Stamp, J. Strachan, P. de Vris, and JET EFDA Contributors, Plasma Phys. Control. Fusion **46**, A87 (2004).

[7] Y. Martin, R. Behn, I. Furno, B. Labit, H. Reimerdes, and the TCV Team, Nucl. Fusion **54**, 114006 (2014).

[8] Y. Ma, J. W. Hughes, A. E. Hubbard, B. LaBombard, R. M. Churchill, T. Golfinopolous, N. Tsuji, and E. S. Marmar, Nucl. Fusion **52**, 023010 (2012).

[9] C. F. Maggi, E. Delabie, T. M. Biewer, M. Groth, N. C. Hawkes, M. Lehnen, E. de la Luna, K. McCormick, C. Reux, F. Rimini, E. R. Solano, Y. Andrew, C. Bourdelle, V. Bobkov, M. Brix, G. Calabro, A. Czarnecka, J. Flanagan, E. Lerche, S. Marsen, I. Nunes, D. Van Eester, M. F. Stamp, and JET EFDA Contributors, Nucl. Fusion **54**, 023007 (2014).

[10] F. Ryter, S. K. Rathgeber, Orte L. Barrera, M. Bernert, G. D. Conway, R. Fischer, T. Happel, B. Kurzan, R. M. McDermott, A. Scarabosio, W. Suttrop, E. Viezzer, M. Willensdorfer, E. Wolfrum, and the ASDEX Upgrade Team, Nucl. Fusion **53**, 113003 (2013).

[11] L. M. Shao, E. Wolfrum, F. Ryter, G. Birkenmeier, F. M. Laggner, E. Viezzer, R. Fischer, M. Willensdorfer, B. Kurzan, T. Lunt, and the ASDEX Upgrade Team, Plasma Phys. Control. Fusion **58**, 025004 (2016).

[12] S. M. Kaye, R. Maingi, D. Battaglia, R. E. Bell, C. S. Chang, J. Hosea, H. Kugel, B. P. LeBlanc, H. Meyer, G. Y. Park, and J. R. Wilson, Nucl. Fusion **51**, 113019 (2011).

[13] D. J. Battaglia, C. S. Chang, S. M. Kaye, K. Kim, S. Ku, R. Maingi, R. E. Bell, A. Diallo, S. Gerhardt, B. P. LeBlanc, J. Menard, M. Podesta, and the NSTX Team, Nucl. Fusion **53**, 113032 (2013).

[14] G. S. Xu, H. Q. Wang, M. Xu, B. N. Wang, H. Y. Guo, P. H. Diamond, G. R. Tynan, R. Chen, N. Yan, D. F. Kong, H. L. Zhao, A. D. Liu, T. Lan, V. Naulin, A. H. Nielsen, J. Juul Rasmussen, K. Miki, P.

Manz, W. Zhang, L. Wang, L. M. Shao, S. C. Liu, L. Chen, S. Y. Ding, N. Zhao, Y. L. Li, Y. L. Liu, G. H. Hu, X. Q. Wu, and X. Z. Gong, Nucl. Fusion **54**, 103002 (2014).

[15] F. Wagner, G. Fussmann, T. Grave, M. Keilhacker, M. Kornherr, K. Lackner, K. McCormick, E. R. Müiller, A. Stäbler, G. Becker, K. Bernhardi, U. Ditte, A. Eberhagen, O. Gehre, J. Gernhardt, G. v. Gierke, E. Gruber, G. Haas, M. Hesse, G. Janeschitz, F. Karger, S. Kissel, O. Klüber, G. Lisitano, H. M. Mayer, D. Meisel, V. Mertens, H. Murmann, W. Poschenrieder, H. Rapp, H. Röhr, F. Ryter, F. Schneider, G. Siller, P. Smeulders, F. Söldner, E. Speth, K. H. Steuer, Z. Szymanski, and O. Vollmer, Phys. Rev. Lett. **53**, 1453 (1984).

[16] T. Ido, K. Kamiya, Y. Miura, Y. Hamada, A. Nishizawa, and Y. Kawasumi, Phys. Rev. Lett. **88**, 055006 (2002).

[17] Y. R. Martin and TCV team, Plasma Phys. Control. Fusion **46**, 8 (2004).

[18] K. J. Zhao, J. Cheng, P. H. Diamond, J. Q. Dong, L. W. Yan, W. Y. Hong, M. Xu, G. Tynan, K. Miki, Z. H. Huang, K. Itoh, S. I. Itoh, A. Fujisawa, Y. Nagashima, S. Inagaki., Z. X. Wang, L. Wei, X. M. Song, G. J. Lei, Q. Li, X. Q. Ji, Yi Liu, Q. W. Yang, X. T. Ding, and X. R. Duan, Nucl. Fusion **53**, 123015 (2013).

[19] J. D. Callen and G. L. Jans, Phys. Rev. Lett. **38**, 491 (1977).

[20] M. Soler and J. D. Callen, Nucl. Fusion **19**, 703 (1979).

[21] E. D. Fredrickson, M. E. Austin, R. Groebner, J. Manickam, B. Rice, G. Schmidt, and R. Snider, Phys. Plasmas **7**, 5051 (2000).

[22] E. D. Fredrickson, K. McGuire, A. Cavallo, R. Budny, A. Janos, D. Monticello, Y. Nagayama, W. Park, G. Taylor, and M. C. Zarnstorff, Phys. Rev. Lett. **65**, 2869 (1990).

[23] A. J. Creely, A. E. White, E. M. Edlund, N. T. Howard, and A. E. Hubbard, Nucl. Fusion **56**, 036003 (2016).

[24] F. De Luca, P. Galli, G. Gorini, A. Jacchia, P. Mantica, N. Deliyanakis, M. Erba, and L. Porte, Nucl. Fusion **36**, 909 (1996).

[25] B. Geiger, M. Garcia-Munoz, R. Dux, F. Ryter, G. Tardini, L. Barrera Orte, I. G. J. Classen, E. Fabke, R. Fischer, V. Igochine, R. M. McDermott, and the ASDEX Upgrade Team, Nucl. Fusion **54**, 022005 (2014).

[26] P. Sauter, T. Pütterich, F. Ryter, E. Viezzer, E. Wolfrum, G. D. Comway, R. Fischer, B. Kurzan, R. M. McDermott, S. K. Rathgeber, and the ASDEX Upgrade Team, Nucl. Fusion **52**, 012001 (2012).

[27] M. Cavedon, T. Pütterich, E. Viezzer, G. Birkenmeier, T. Happel, F. M. Laggner, P. Manz, F. Ryter, U. Stroth, and The ASDEX Upgrade Team, Nucl. Fusion **57**, 014002 (2017).

[28] F. Ryter, L. Barrera Orte, B. Kurzan, R. M. McDermott, G. Tardini, E. Viezzer, M. Bernert, R. Fischer, and The ASDEX Upgrade Team, Nucl. Fusion **54**, 083003 (2014).

[29] Eun-jin Kim and P. H. Diamond, Phys. Rev. Lett. **90**, 185006 (2003).

[30] G. S. Xu, B. N. Wan, H. Y. Guo, H. L. Zhao, A. D. Liu, V. Naulin, P. H. Diamond, G. R. Tynan, M. Xu, R. Chen, M. Jiang, P. Liu, N. Yan, W. Zhang, L. Wang, S. C. Liu, and S. Y. Ding, Phys. Rev. Lett. **107**, 125001 (2011).

[31] G. D. Conway, C. Angioni, F. Ryter, P. Sauter, J. Vicente, and ASDEX Upgrade Team, Phys. Rev. Lett. **106**, 065001 (2011).

[32] Z. Yan, G. R. McKee, R. Fonck, P. Gohil, R. J. Groebner, and T. H. Osborne, Phys. Rev. Lett. **112**, 125002 (2014).

[33] I. Cziegler, G. R. Tynan, P. H. Diamond, A. E. Hubbard, J. W. Hughes, J. Irby, and J. L. Terry, Nucl. Fusion **55**, 083007 (2015).

[34] M. A. Malkov, P. H. Diamond, K. Miki, J. E. Rice, and G. R. Tynan, Phys. Plasmas **22**, 032506 (2015).

[35] G. R. Tynan, I. Cziegler, P. H. Diamond, M. Malkov, A. Hubbard, J. W. Hughes, J. L. Terry, and J. H. Irby, Plasma Phys. Control. Fusion **58**, 044003 (2016).

[36] L. Schmitz, Nucl. Fusion **57**, 025003 (2017).

[37] G. R. Tynan, M. Xu, P. H. Diamond, J. A. Boedo, I. Cziegler, N. Fedorczak, P. Manz, K. Miki, S. Thakur, L. Schmitz, L. Zeng, E. J. Doyle, G. M. McKee, Z. Yan, G. S. Xu, B. N. Wan, H. Q. Wang,

H. Y. Guo, J. Dong, K. Zhao, J. Cheng, W. Y. Hong, and L. W. Yan, Nucl. Fusion **53**, 073053 (2013).
[38] I. Cziegler, G. R. Tynan, P. H. Diamond, A. E. Hubbard, J. W. Hughes, J. Irby, and J. L. Terry, Plasma Phys. Control. Fusion **56**, 075013 (2014).
[39] C. S. Chang, S. Ku, G. R. Tynan, R. Hager, R. M. Churchill, I. Cziegler, M. Greenwald, A. E. Hubbard, and J. W. Hughes, Phys. Rev. Lett. **118**, 175001 (2017).
[40] J. C. Hillesheim, E. Delabie, H. Meyer, C. F. Maggu, L. Meneses, E. Poli, and JET Contributors EUROfusion Consortium, JET, Culham Science Centre, Abingdon, Oxon OX14 3DB, United Kingdom, Phys. Rev. Lett. **116**, 065002 (2016).
[41] P. Manz, G. S. Xu, B. N. Wan, H. Q. Wang, H. Y. Guo, I. Cziegler, N. Fedorczak, C. Holland, S. H. Müller, S. C. Thakur, M. Xu, K. Miki, P. H. Diamond, and G. R. Tynan, Phys. Plasmas **19**, 072311 (2012).
[42] M. Shimada, D. J. Campbell, V. Mukhovatov, M. Fujiwara, N. Kirneva, K. Lackner, M. Nagami, V. D. Pustovitov, N. Uckan, J. Wesley, N. Asakura, A. E. Costley, A. J. H. Donné, E. J. Doyle, A. Fasoli, C. Gormezano, Y. Gribov, O. Gruber, T. C. Hender, W. Houlberg, S. Ide, Y. Kamada, A. Leonard, B. LIpschultz amd A. Loarte, K. Miyamoto, V. MUkhovatov, T. H. Osborne, A. Polevoi, and A. C. C. Sips, Nucl. Fusion **47**, S1 (2007).
[43] Yanmin DUAN, Liqun HU, Songtao MAO, Ping XU, Kaiyun CHEN, Shiyao LIN, Guoqiang ZHONG, Jizong ZHANG, Ling ZHANG, and Liang WANG, Plasma Sci. Technol. **13**, 546 (2011).
[44] W. Zhang, J. F. Chang, B. N. Wan, G. S. Xu, C. J. Xiao, B. Li, G. S. Xu, N. Yan, L. Wang, S. C. Liu, M. Jiang, and P. Liu, Rev. Sci. Instrum. **81**, 113501 (2010).
[45] L. M. Shao, G. S. Xu, R. Chen, L. Chen, G. Birkenmeier, Y. M. Duan, W. Gao, P. Manz, T. H. Shi, H. Q. Wang, L. Wang, M. Xu, N. Yan, L. Zhang, and the EAST Team, Plasma Phys. Control. Fusion **60**, 035012 (2018).
[46] K. Itoh and S-I. Itoh, Plasma Phys. Control. Fusion **38**, 1 (1996).
[47] T. Kobayashi, K. Itoh, T. Ido, K. Kamiya, S. I. Itoh, Y. Miura, Y. Nagashima, A. Fujisawa, S. Inagaki, K. Ida, and K. Hoshino, Phys. Rev. Lett. **111**, 035002 (2013).
[48] G. Birkenmeier, M. Cavedon, G. D. Conway, P. Manz, U. Stroth, R. Fischer, G. Fuchert, T. Happel, F. M. Laggner, M. Maraschek, A. Medvedeva, V. Nikolaeva, D. Prisiazhniuk, T. Pütterich, F. Ryter, L. M. Shao, M. Willensdorfer, E. Wolfrum, H. Zohm, and the ASDEX Upgrade Team, Nucl. Fusion **56**, 086009 (2016).
[49] K. Miki, P. H. Diamond, Ö. D. Gürcan, G. R. Tynan, T. Estrada, L. Schmitz, and G. S. Xu, Phys. Plasmas **19**, 092306 (2012).
[50] J. M. Beall, Y. C. Kim, and E. J. Powers, J. Appl. Phys. **53**, 3933 (1982).
[51] S. J. Levinson, Nucl. Fusion **24**, 527 (1984).